J Solid State Electrochem (2016) 20:1397–1404
DOI 10.1007/s10008-016-3134-6

ORIGINAL PAPER

Carbon/titanium oxide supported bimetallic platinum/iridium nanocomposites as bifunctional electrocatalysts for lithium-air batteries

Awan Zahoor[1] · Maria Christy[2] · Yongbin Kim[3] · Anupriya Arul[3] · Yun Sung Lee[4] · Kee Suk Nahm[2,3]

Received: 24 September 2015 / Revised: 9 January 2016 / Accepted: 19 January 2016 / Published online: 5 February 2016

Abstract Platinum (Pt) and iridium (Ir) catalysts are well known to strongly enhance the oxygen reduction reaction (ORR) and oxygen evolution reaction (OER) kinetics, respectively. Pt–Ir-based bimetallic compounds along with carbon-supported titanium oxides (C–TiO_2) have been synthesized for the application as electrocatalysts in lithium oxygen batteries. Transition metal oxide-based bimetallic nanocomposites (Pt–Ir/C–TiO_2) were prepared by an incipient wetness impregnation technique. The as-prepared electrocatalysts were composed of a well-dispersed homogenous alloy of nanoparticles as confirmed by X-ray diffraction patterns and Fourier transform scanning electron microscopy analyses. The electrochemical characterizations reveal that the Pt–Ir/C–TiO_2 electrocatalysts were bifunctional with high activity for both ORR and OER. When applied as an air cathode catalyst in lithium-air batteries, the electrocatalyst improved the battery performance in terms of capacity, reversibility, and cycle life compared to that of cathodes without any catalysts.

✉ Yun Sung Lee
leeys@chonnam.ac.kr

✉ Kee Suk Nahm
nahmks@jbnu.ac.kr

[1] Department of Chemical Engineering, N.E.D. University of Engineering and Technology, University Road, Karachi 75270, Pakistan

[2] R&D Education Centre for Fuel Cell Materials & Systems, Chonbuk National University, Jeonju 561-756, Republic of Korea

[3] Department of Semiconductor and Chemical Engineering, Chonbuk National University, Jeonju 561-756, Republic of Korea

[4] Faculty of Applied Chemical Engineering, Chonnam National University, Gwangju 500-757, Republic of Korea

Keywords Air cathodes · Bimetallic catalysts · Bifunctional electrocatalysts · Lithium-air batteries · Nanocomposites

Introduction

Lithium oxygen (Li–O_2) batteries had been considered to be promising alternative power sources of future electric vehicles [1–5]. However, the poor activity of electrocatalysts and the slow reaction kinetics had kept them far from reality. The main issues that affect the electrochemical performance of Li–O_2 batteries included charge overpotential and low rate capability [4, 5]. The overall discharge–charge processes of the battery could be explained as oxygen reduction reaction (ORR) and oxygen evolution reaction (OER), respectively. The solid discharge products, Li_2O_2, formed during discharging should be electrochemically decomposed to Li and O_2 on recharge. However, this might not be the case always where formation of undesired intermediate species other than Li_2O_2 could happen due to the unsolicited side reactions between Li superoxide and ORR products [6–8]. So in order to promote the proper formation and decomposition of Li_2O_2, bifunctional electrocatalysts are utilized. However, key limitations of commercially available precious metal electrocatalysts such as Pt, Pd, Ru, and Ir include high cost and unavailability. Noble metals represent the fifth and sixth period, group 8B elements in the periodic table, and these elements are known as excellent catalysts for many chemical reactions. Owing to their high catalytic activity and keeping in mind the major limitations of these catalysts, it is important to significantly reduce the amount of these precious metals and yet achieve the maximum bifunctional activity. This could be achieved by designing a perfectly suited or optimizing the catalyst with metal oxides, thus minimizing the mass and maximizing the efficiency [9–12].

Platinum (Pt) is considered as a nearly ideal catalyst for oxygen reduction reaction which is still being widely used [13, 14]. Alloying Pt with other metals (M), Pt/M is a viable approach to obtain bifunctional electrocatalytic activity, that is, to catalyze both ORR and OER in the air cathode. Neyerlin and co-workers [15] have studied the combinatorial array which demonstrated the reliable trends in electrocatalytic activity mainly for oxygen evolution reaction based on Pt–metal binary electrocatalysts. According to the authors [15], alloys of iridium (Ir) showed improved OER activity [16]. Recent reports [17, 18] have also shown that bimetallic or binary electrocatalysts exhibit improved catalytic activity for ORR and OER than pure metal catalysts. Pt being the better suited candidate for ORR catalysts and Ir being one of the most promising OER catalysts, bimetallic Pt/Ir could be the ideal candidate for a bifunctional electrocatalyst. However, since both Pt and Ir are expensive metals, designing suitable bimetallic catalysts with appropriate catalyst support could minimize the utilization of pure metals. In that case, a metal oxide-based support might help to serve the original purpose of designing a bifunctional catalyst with minimal utilization for maximum efficiency.

Titanium oxides (TiO_2) had been one of the most broadly studied metal oxides in the field of energy conversion and storage due to its superior physicochemical properties, excellent stability, and low cost for synthesis and its being environmentally friendly and biocompatible [19, 20]. TiO_2 is an attractive catalyst support, and according to Bruce et al. [21], it could improve the highest occupied molecular orbital spatial size of noble metals and weaken the adsorption of atomic oxygen on catalysts, which is significant for improving the catalytic ability of electrocatalysts [22].

Another feasible approach to reduce the amount of noble metal catalysts is the usage of carbon supports that could provide a high surface area and stabilize the initial catalyst surface area, and thereby the mass-based activity of the catalyst itself [23–26]. Carbon nanomaterials were an efficient support for nanometal catalysts and there had been various types of carbon supports. Amongst them, high surface area Vulcan XC–72 carbon had been preferred as a catalyst support material. Hence, both transition metal oxide (TiO_2) and Vulcan carbon (C) support, hereafter known as C–TiO_2, had been utilized to synthesize bimetallic Pt–Ir nanocomposites. That is, Pt–Ir/C–TiO_2 catalysts were synthesized and investigated as bifunctional electrocatalysts for an air cathode of Li–O_2 batteries in this work.

Herein, bimetallic Pt/Ir nanocomposites on a C–TiO_2 support have been investigated as bifunctional electrocatalysts for Li–O_2 batteries. The Pt–Ir/C–TiO_2 catalysts were synthesized using incipient wetness impregnation synthesis. Pt and Ir catalysts were also synthesized separately on the C–TiO_2 support in order to investigate the ORR and OER activities using cyclic voltammetry and galvanostatic battery testing. To the best of our knowledge, there were not much previous reports on this unique combination of bimetallic catalyst on C–TiO_2. The C–TiO_2 support seemed to be a stable support providing high electronic conductivity. Pt/C–TiO_2 proved to be an efficient catalyst for ORR as a Ir/C–TiO_2 catalyst for OER. Together, Pt–Ir/C–TiO_2 exhibited bifunctional catalytic activity for both ORR and OER. The Pt–Ir/C–TiO_2 bifunctional catalysts, when applied as an air cathode catalyst of Li–O_2 batteries, showed excellent performance with high capacity and cyclability and reduced voltage gap, compared to batteries with no catalysts. From this study, it is evident that Pt–Ir/C–TiO_2 constitutes an effective catalyst with significant performance for ORR and OER activities.

Experimental

All the chemicals were commercially purchased and used without further purification. Carbon materials were purchased from Carbon Nanomaterial Technology, Co., Ltd.

Synthesis and characterizations

To obtain a C–TiO_2 compound, 400 mg of Vulcan carbon and 60 mg of TiO_2 were dispersed and dissolved, respectively, in that order in 300 ml of isopropyl alcohol solution and sonicated for 30 min. The mixed solution was then placed on oil bath at 60 °C while 1 ml deionized water was added to it and the mixture was stirred continuously for 1 h. The final product was filtered and dried at 80 °C under vacuum overnight. The samples were annealed at 600 °C under N_2 atmosphere for 2 h at a rate of 5 °C min^{-1}.

To prepare C–TiO_2-supported Pt/Ir bimetallic nanocomposites, equal weight percentages of Pt and Ir were used. For the synthesis, 75 mg (0.23 mmol) of $IrCl_3 \cdot H_2O$ and 122 mg (0.23 mmol) of $H_2PtCl_6 \cdot 6H_2O$ were dispersed in 6 and 10 ml of DI water, respectively. 1 M aqueous KOH solution was prepared by adding 5.6 g of KOH in 100 ml of DI water. This solution was added dropwise until a pH of 12 is obtained. Finally, 87 mg (five times of the total metal precursors present in solution, 2.3 mmol) of $NaBH_4$ dissolved in 20 ml of DI water was added to the mixture. The mixture was stirred continuously for 4 h at 120 °C to completely reduce the metal ions. After the reduction process, 5 M HCl was added dropwise to adjust the pH to 3 and the mixture is cooled at room temperature. Centrifugation was performed at 4000 rpm for 15 min, and this step was repeated for at least four times with fresh DI water. Initial drying was under vacuum at 70 °C for 2 h, after which annealing was done at 250 °C under H_2 and N_2 (1:9 volume) atmospheres for 2 h at a rate of 5 °C min^{-1}. The same procedure with negligible adjustment was utilized to synthesize Pt/C–TiO_2 and Ir/C–TiO_2 separately with respective precursors.

The phase structures of the as-prepared samples were determined by X-ray powder diffraction (XRD, Shimadzu XRD–6000, Cu KR, λ 1.5406 Å) at a scanning rate of 1° min^{-1}. The morphology of the as-prepared catalyst materials was examined by field emission scanning electron microscopy (FESEM, JSM–6700F) and high-resolution transmission electron microscopy (HRTEM, JEM–2010, JEOL).

Electrochemical characterizations

The electrocatalytic activity of the samples was evaluated by measuring ORR and OER polarization curves using cyclic voltammetry (CV) and rotating ring–disk electrode (RRDE) voltammetry. The electrochemical studies were carried out using a computer-controlled potentiostat (CHI 760D, CH Instrument) equipped with a typical three-electrode cell. A Pt wire and Hg/HgO were used as the counter and reference electrodes, respectively, in the test cell. O_2 was bubbled directly into the cell for at least an hour prior to the electrochemical measurements. For CV, the working electrode was scanned between −0.8 and 0.3 V at a sweep rate of 50 mV s^{-1} after the electrolyte was saturated with pure oxygen. For LSV, the working electrode was recorded in the potential ranges of 0.3 to −0.8 V and 0.3 to 1.0 V for ORR and OER, respectively, in oxygen-saturated 0.1 M KOH solution at a scan rate of 5 mV s^{-1} and a disk rotation rate of 1600 rpm. The CV studies were performed in both aqueous and organic media. For CV in the organic medium, the electrocatalytic activity of the air cathodes was analyzed using Swagelok™-type cells in a non-aqueous LiTFSI (TEGDME) electrolyte with MultiStat computer-controlled program.

For ORR studies, the synthesized Pt–Ir/C–TiO_2 catalyst was mixed with carbon powder (Cabot Vulcan XC–72) at a weight ratio of 3:7 to ensure sufficient electronic conductivity. Five milligrams of the as-prepared catalyst was dispersed ultrasonically in 75 μl of diluted Nafion alcohol solution (5 wt%), and about 20 μl of the suspension was pipetted onto a glassy carbon substrate. For comparison, a commercial Pt/C (Vulcan XC–72) electrode was also analyzed for ORR and OER performance under the same experimental procedures.

The Li–O_2 cell performance was tested galvanostatically under oxygen flow (10 cm^3 min^{-1}) in a potential window of 2 to 4.3 V in a BTS 2004 (Japan) battery tester at different current densities (0.1–0.3 mA cm^{-2}). The performance of the Pt–Ir/C–TiO_2 catalyst in the Li–O_2 air cathode was evaluated using the Swagelok™-type cells.

For lithium-air battery studies, the air cathodes were prepared by mixing the as-prepared Pt–Ir/C–TiO_2 catalyst and Ketjen black (EC 600JD) conductive carbon at a ratio of 1:2 with a teflonized acetylene black (TAB) binder (60 %) in isopropyl alcohol. The mixture was prepared into a fine pellet of about 1 cm diameter and pressed on a Ni mesh current collector of 1.2 cm diameter. Thus, the prepared electrode was then dried in vacuum overnight at 100 °C and used as the air cathode in the Li-air battery. A Li foil was used as the anode; our prepared electrode (as mentioned above in "Electrochemical characterizations") was used as the cathode, and 1 M LiTFSI (TEGDME) was employed as the electrolyte. TEGDME-based electrolytes have been used in this study because they have been reported to be relatively stable, less volatile, and more conductive than other carbonate-based electrolytes in air batteries [27–29]. These electrolytes are also reported to possess substantially higher stability than carbonates as they are less susceptible to nucleophilic substitution by superoxide anion radicals and are stable against oxidation potentials up to 4.5 V vs. Li/Li^+ unless in the presence of Li_2O_2. A potential window of 2 to 4.3 V had been utilized in this study mainly because the decomposition voltage of TEGDME was determined to be above 4.3 V [30, 31].

Result and discussions

Structural characterization

Pt/Ir nanocomposites supported on TiO_2 and Vulcan carbon were synthesized by an incipient wetness impregnation technique. The XRD spectra of Pt/Ir nanocomposites supported on C–TiO_2 are shown in Fig. 1. For comparison, the XRD spectrum of commercial Pt/C is also included in Fig. 1. The XRD spectrum of Vulcan carbon showed two broad diffraction peaks at 25° and 43.2° corresponding to (002) and (101) planes of hexagonal graphite (JCPDS 75–1621) [32]. The broadening

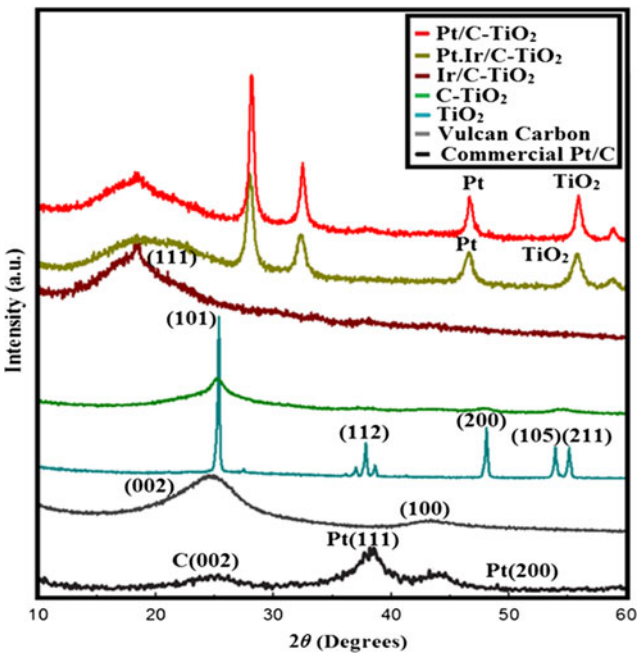

Fig. 1 The XRD spectra of Pt/Ir nanocomposites supported on C–TiO_2

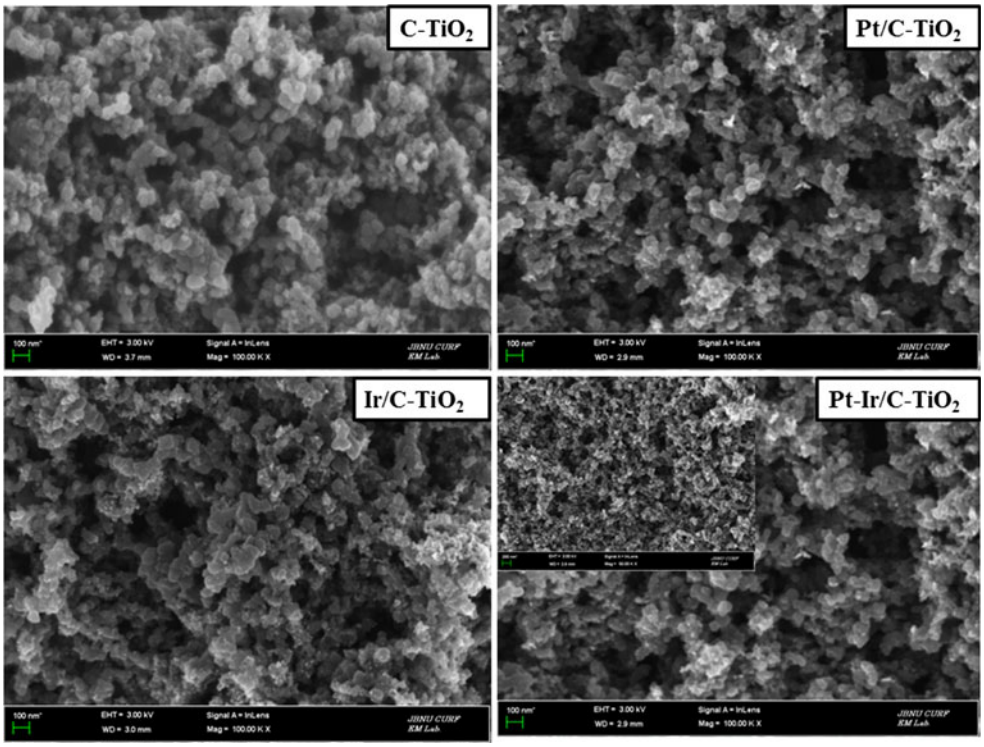

Fig. 2 FESEM images of C–TiO_2 and Pt, Ir, and Pt/Ir nanocomposites supported on C–TiO_2

of the peaks showed the amorphous nature of the Vulcan carbon materials. The XRD patterns of TiO_2 exhibited strong peaks at 26°, 36°, 48°, and 55° that are in good agreement with the standard spectrum (JCPDS 88–1175 and 84–1286) [33]. The characteristic diffraction peaks of Pt at 38°, 68°, and 82° corresponded to (111), (220), and (311) planes, respectively, which is in accordance with JCPDS 001–1190; Ir could be indexed to (111) and (220) at 68 and 82, respectively (JCPDS 006–0598). The broad peaks implied a small particle size and low degree of crystallinity.

The nanoparticle structure was examined using scanning electron microscopy and the images are given in Fig. 2. As observed from Fig. 2, the C–TiO_2 mixture showed densely arranged and smooth-surfaced irregular spherical particles. The average size of the particles varied between 50 and 100 nm. The distribution of Pt, Ir, and Pt/Ir nanoparticles on the surface of C–TiO_2 caused the surface to appear rough and sharp (Fig. 2). The average particle sizes of the nanomaterials ranged between 50 and 52, 28 and 40, and 48 and 50 nm for Pt/C–TiO_2, Ir/C–TiO_2, and Pt–Ir/C–TiO_2, respectively. To confirm the uniform deposition of nanoparticles on C–TiO_2, transmission electron microscopy was also performed on Pt–Ir/C–TiO_2 materials, which could be seen in Fig. 3. From Fig. 3a, it can be observed that the Pt/Ir nanomaterials have been uniformly distributed in the C–TiO_2 carpet without any aggregation. Figure 3b shows a high-resolution micrograph of various single particles and interlaced lattice fringes of the Pt/Ir alloy. The distance between two planes was measured to be 0.34 nm which is in accordance with the XRD *d* spacing value of planes (101) of TiO_2 and (002) of carbon. The two other *d* values calculated by HRTEM to be 0.2 and 0.19 nm were in agreement with XRD results in Fig. 1, confirming the distributed particles to be Pt and Ir.

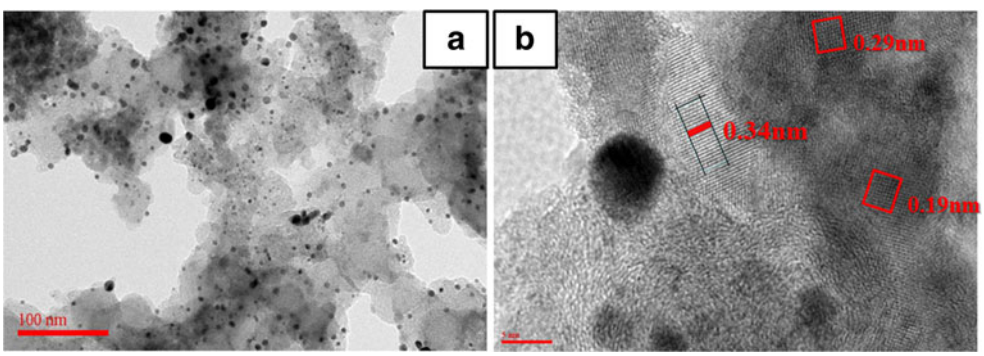

Fig. 3 **a**, **b** HRTEM images of Pt/Ir nanocomposites supported on C–TiO_2

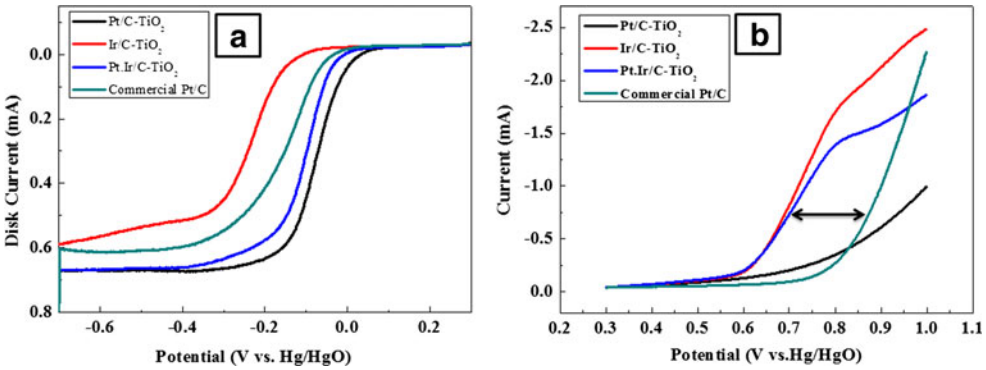

Fig. 4 **a**, **b** LSV curves of Pt–Ir/C–TiO_2 nanocomposites at 1600 rpm in 0.1 M KOH saturated with oxygen at a potential scan rate of 5 mV s^{-1}

Electrochemical characterization

The electrocatalytic activities of Pt–Ir/C–TiO_2 were evaluated by various electrochemical techniques. The rotating ring–disk electrode was used at 1600 rpm in 0.1 M KOH saturated with oxygen at a potential scan rate of 5 mV s^{-1} to investigate the ORR and OER characteristics of Pt–Ir/C–TiO_2 by linear sweep voltammetry. As seen in Fig. 4a, b, Pt/C–TiO_2 exhibited better ORR activity with a positively shifted reduction peak and Ir/C–TiO_2 exhibited better OER activity with a negatively shifted oxidation peak. Pt–Ir/C–TiO_2 exhibited superior electrocatalytic activity for both ORR and OER better than commercial Pt/C. The onset potential and half-wave potential values from Fig. 4 are summarized in Table 1. The corresponding Koutecky–Levich (KL) plot was utilized and the electron transfer number per oxygen molecule (n) during ORR was calculated by the equation

$$n = \frac{4I_D}{I_D + \frac{I_R}{N}} \quad (1)$$

where I_D, I_R, and N are the disk current, ring current, and ring collection efficiency (here $N = 0.37$), respectively [30]. The calculated electron transfer numbers were 3.9, 3.7, and 3.8 for Pt/C–TiO_2, Ir/C–TiO_2, and Pt–Ir/C–TiO_2, respectively, as given in Table 1. From these values, it is clear that these catalysts undergo quasi four-electron transfer which is desired for better electrocatalytic performance in ORR.

Table 1 Electrochemical data obtained from the LSV curves in Fig. 4

S. no.	Sample	Electron transfer number (n)	ORR		OER	
			Onset potential (V)	Half-wave potential (V)	Onset potential (V)	Half-wave potential (V)
1	Pt/C–TiO_2	3.90	−0.007	−0.08	0.79	0.86
2	Ir/C–TiO_2	3.70	−0.15	−0.23	0.58	0.74
3	Pt–Ir/C–TiO_2	3.57	−0.03	−0.10	0.58	0.86
4	Commercial Pt/C	3.72	−0.06	0.14	0.71	0.91

The cyclic voltammogram of Pt–Ir/C–TiO_2 in 0.1 M KOH saturated with oxygen at a potential scan rate of 5 mV s^{-1} could be seen in Fig. 5a. The strong reduction peaks observed in Fig. 5a for all the synthesized materials were comparable to those for the commercial Pt/C catalyst measured under the same experimental conditions. Pt–Ir/C–TiO_2 shows superior performance with a positively shifted reduction peak than that of Pt/C–TiO_2 and Ir/C–TiO_2 and closer to that of commercial Pt/C. The reduction peak potential of Pt–Ir/C–TiO_2 is measured to be 0.08 V. This signifies the electrocatalytic activity of Pt–Ir/C–TiO_2 towards the oxygen cathode region. Followed by Pt–Ir/C–TiO_2, Pt/C–TiO_2 also exhibits a positively shifted peak with the reduction peak potential (−0.14 V).

So far, every catalyst that has been used in air cathodes with non-aqueous electrolytes had been proven efficient for ORR and OER in aqueous phase [18, 34–36]. However, in order to understand the behavior of the Pt–Ir/C–TiO_2 catalyst in non-aqueous electrolytes, the cyclic voltammogram of Pt–Ir/C–TiO_2-catalyzed Li-air batteries was analyzed in LiTFSI (TEGDME) electrolytes. The CV curves of all the cells were recorded in the range of 1.5 to 4.7 V vs. Li at a scan rate of 0.01 mV s^{-1} as given in Fig. 5b. As seen in Fig. 5b, the CV of Pt–Ir/C–TiO_2 in the oxygen-saturated electrolyte solution exhibited a sharp reduction peak at an ORR potential of 2.56 V with high peak current. This sharp reduction peak indicated the formation of Li_2O_2 by the ORR. During anodic scan, Pt–Ir/C–TiO_2 exhibited a sharp yet smaller anodic peak at the OER potential of 4.3 V. The thin invisible peaks around 3.4 V must be due to the rapid reaction kinetics and account to the oxidation of LiO_2 formed during the chemical reduction of the Li and O_2 during Li_2O_2 formation reaction. Also, the LiO_2 and O^{2-} remaining in the electrolyte get reduced at this potential [37, 38]. The

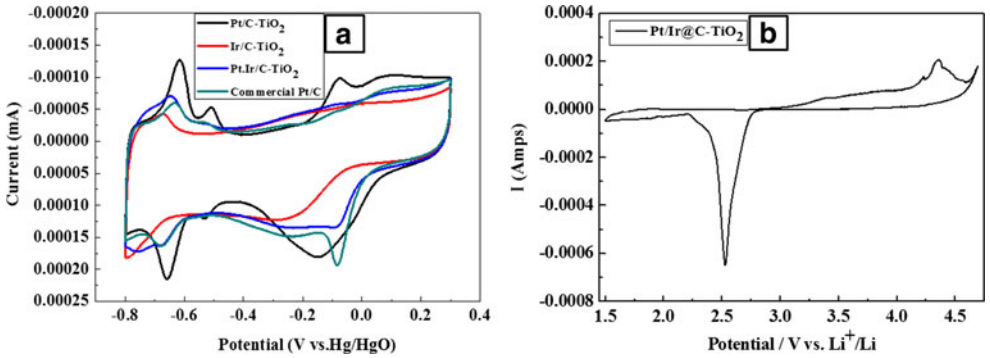

Fig. 5 **a** Cyclic voltammograms of Pt/Ir nanocomposites supported on C–TiO_2 in 0.1 M KOH saturated with oxygen at a potential scan rate of 5 mV s^{-1}. **b** Cyclic voltammograms of Pt/Ir nanocomposites supported on C–TiO_2 in non-aqueous 1 M LiTFSI (TEGDME) electrolyte

ORR and OER peak potentials well matched with the Li_2O_2 formation and decomposition potentials of the Li-air battery with the Pt–Ir/C–TiO_2 catalyst.

Li battery application

The performance of the Pt–Ir/C–TiO_2 catalysts in Li–O_2 batteries was evaluated with 1 M LiTFSI in TEGDME as the electrolyte in Swagelok-type cells. The charge–discharge cycles were measured under an oxygen pressure of 1 atm and a constant current density of 0.1 mA in the potential window of 2.0–4.3 V. Figure 6 shows the first discharge capacity of the Pt–Ir/C–TiO_2 catalyst in comparison with a KB cathode without any catalyst. The Pt–Ir/C–TiO_2-catalyzed air cathode exhibited a first discharge capacity of 4375 mAh g^{-1}, which was double that of the KB cathode with 2150 mAh g^{-1}. The first discharge capacities of Pt/C–TiO_2 and Ir/C–TiO_2 were measured to be 3856 and 3600 mAh g^{-1}, respectively. The Pt/C–TiO_2-catalyzed cell exhibited poor reversibility with less capacity retention (53 %) upon charging, since the Pt-based catalyst exhibited better ORR activity but poor OER activity. The high oxygen evolution overpotential and formation of a stable surface oxide

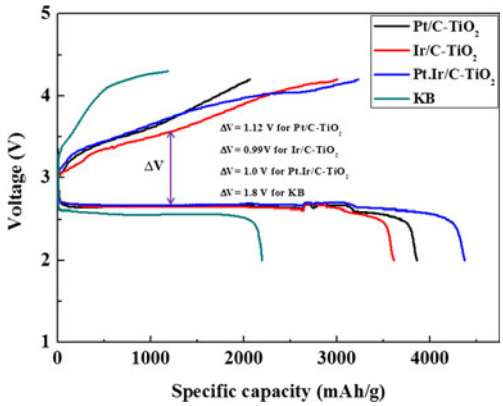

Fig. 6 The first discharge capacity of Pt, Ir, and Pt–Ir/C–TiO_2 catalysts in comparison with the KB cathode

layer in Pt catalysts impeded their OER activity since the charge process might require much higher potential [39, 40]. But at a lower OER overpotential, Pt would suffer less oxidation which improves the active Pt surface for ORR. On the other hand, in Ir/C–TiO_2, >85 % reversibility was obtained with the first charge capacity of 3100 mAh g^{-1} since the Ir-based catalyst exhibited better OER activity. Overall, as expected, Pt–Ir/C–TiO_2 delivered better performance with high capacity and 86 % capacity retention than Pt- and Ir-based catalysts. Ir-based catalysts revealed comparable numbers of surface sites for nanoparticles that proved to be electrochemically active for OER reactions [41]. As effective OER catalysts, Ir-based catalysts decreased the charging overpotential and protected Pt from overoxidation. Consequently, the cell exhibited a much improved discharge performance with the Pt–Ir/C–TiO_2 bifunctional catalyst. The performance of the Pt–Ir/C–TiO_2-catalyzed battery, and for that matter all synthesized cathodes, was much better than that of the KB-only cathode (Fig. 6). The synthesized bimetallic nanomaterial-catalyzed cells exhibited a discharge voltage of 2.6 V whereas the KB cathode exhibited 2.5 V. The synthesized catalysts had significantly reduced the charge overpotential of the batteries. In detail, the charge voltage of Ir/C–TiO_2 and Pt–Ir/C–TiO_2 was better than that of Pt/C–TiO_2, which once again confirmed the OER activity of Ir-based catalysts. The overpotential (ΔV) of all the catalysts is given in Fig. 6. The superior performance of the Pt–Ir/C–TiO_2-catalyzed Li-air battery could be attributed to the catalysts since Pt and Ir have considerably improved the ORR and OER activities of the cell with proper formation and decomposition of Li_2O_2, respectively.

To investigate the cyclability and reversibility of the synthesized Pt–Ir/C–TiO_2 catalyst, the Li-air batteries were also tested for limited capacity and long cycles. Limiting the cycling capacity will improve the depth of discharge in the battery [42]. Figure 7 shows the cycling performance of Pt/C–TiO_2-, Ir/C–TiO_2-, and Pt–Ir/C–TiO_2-catalyzed Li–O_2 batteries limited at 500 mAh g^{-1} at 0.1 mA cm^{-2}. The discharge

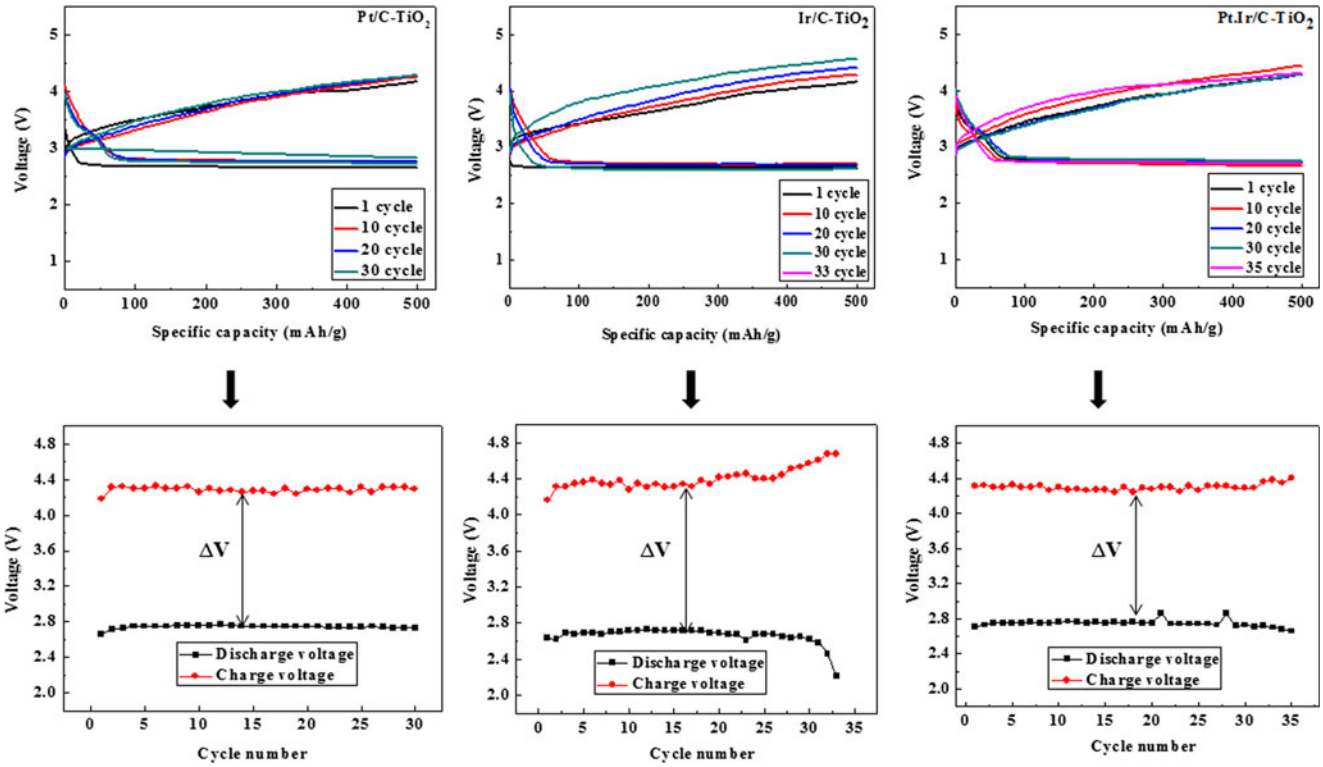

Fig. 7 Cycling performance of the Pt–Ir/C–TiO_2-catalyzed Li–O_2 battery limited to 500 mAh g^{-1}

and charge potential of the cells is also given in Fig. 7 for deeper understanding. There was uniform charge–discharge cycling up to 30 cycles as obtained in Fig. 7 without much increase in the overpotential. Amongst them, Pt–Ir/C–TiO_2 exhibited better performance in terms of overpotential up to 35 cycles. From the above results, it can be perceived that the designing of the Pt–Ir/C–TiO_2 catalyst had been a viable strategy exhibiting enhanced battery performance and at the same time low cost.

It has been well established that the addition of secondary metallic components like iridium enhances the catalytic activity of platinum resulting in bimetallic catalysts [43]. Studies [43, 44] have shown that Pt–Ir bimetallic catalysts exhibit higher and more sustained activity than monometallic platinum catalysts. Thus, in this work, modification of Pt with Ir has significantly improved their catalytic reactivity. From the results, it could be explained that by adjusting the electronic structure and increasing the active facets, the bimetallic Pt/Ir catalysts tend to show great improvements in both activity and stability [45, 46]. Since ORR is very sensitive to the surface electronic properties, that is, coordination of the catalyst, the modification of the surface electronic structure of the catalysts has resulted in the high activity for ORR (and in turn OER with Ir being an excellent OER catalyst). The carbon–TiO_2 support materials, especially with carbon with abundant free-flowing π electrons and a large surface area, improved the stability and durability of the catalyst material [26].

Conclusions

Pt–Ir/C–TiO_2 bifunctional electrocatalysts were synthesized via a simple synthesis technique. High ORR and OER activities for the synthesized Pt–Ir/C–TiO_2 catalyst in both aqueous and non-aqueous electrolyte solutions were obtained. The bifunctional activity of the nanostructure catalyst is almost comparative to or much better than that of commercial Pt/C catalysts. The battery performance is remarkably improved because of the unique combination of the Pt–Ir/C–TiO_2 catalyst. Pt in Pt–Ir/C–TiO_2 has the ability to catalyze ORR and Ir, OER, with fast kinetics and without electrolyte decomposition in the Li–O_2 battery. Pt and Ir improved the reaction kinetics and the C–TiO_2 support rendered a stable structure with better electronic conductivity. With the high cost and scarcity of highly active pure metals, this study revealed that Pt- and Ir-supported nanoparticles could help the future of bifunctional catalysts with minimal utilization and maximum efficiency in battery applications.

Acknowledgments This work was supported by the Human Resources Development program (No. 20114030200060) of the Korea Institute of Energy Technology Evaluation and Planning (KETEP) grant funded by the Korea government Ministry of Trade, Industry and Energy. This work is also supported by the Basic Science Research Program through the National Research Foundation (NRF) funded by the Ministry of Education (No. 2013R1A1A2012656).

References

1. Abraham KM, Jiang Z (1996) J Electrochem Soc 143:1–5
2. Scrosati B, Garche J (2010) J Power Sources 195:2419–2430
3. Bruce PG, Freunberger SA, Hardwick LJ, Tarascon JM (2011) Nat Mater 11:19–29
4. Girishkumar G, McCloskey B, Luntz AC, Swanson S, Wilcke W (2010) J Phys Chem Lett 1:2193–2203
5. Zahoor A, Christy M, Hwang YJ, Nahm KS (2012) J Electrochem Sci Tech 3(1):14–23
6. McCloskey B, Speidel A, Scheffler R, Miller DC, Viswanathan V, Hummelshøj JS, Nørskov JK, Luntz AC (2012) J Phys Chem Lett 3(8):997–1001
7. Black R, Oh SH, Lee JH, Yim T, Adams B, Nazar LF (2012) J Am Chem Soc 134:2902–2905
8. Lu YC, Gallant BM, Kwabi DG, Harding JR, Mitchell RR, Whittingham MS, Horn YS (2013) Energy Environ Sci 6(3): 6750–6768
9. Yu W, Porosoff MD, Chen JG (2012) Chem Rev 112(11):5780–5817
10. Shao Y, Park S, Xiao J, Zhang JG (2012) Wong Y, Liu J. ACS Catal 2:844–857
11. Kim BG, Kim HJ, Back S, Nam KW, Jung Y, Han YK, Choi JW (2014) Scientific Reports 4:4225. doi:10.1038/srep04225
12. Xu JJ, Wang ZL, Xu D, Zhang LL, Zhang XB (2013) Nat Commun 4:2438. doi:10.1038/ncomms3438
13. Liu H, Xing Y (2011) Electrochem Commun 13(6):646–649
14. Lu YC, Gasteiger HA, Parent MC, Chiloyan V, Shao Y (2010) Electrochem Solid State Lett 13:A69–A72
15. Neyerlin KC, Bugosh G, Forgie R, Liu Z, Strasser P (2009) J Electrochem Soc 156:B363–B369
16. Yao W, Yang J, Wang J, Nuli Y (2007) Electrochem Commun 9(5): 1029–1034
17. Jung HY, Park S (2009) Popov BN. J Power Sources 191:357–361
18. Lu YC, Xu Z, Gasteiger HA, Chen S, Hamad-Schifferli K, Shao-Horn Y (2010) J Am Chem Soc 132:12170–12171
19. Zhao G, Mo R, Wang B, Zhang L, Sun K (2014) Chem Mater 26(8):2551–2556
20. Zhu K, Wang Q, Kim JH, Pesaran AA, Frank AJ (2012) J Phys Chem C 116:11895–11899
21. Ottakam Thotiyl MM, Freunberger SA, Peng Z, Chen Y, Liu Z, Bruce PG (2013) Nat Mater 12:1050–1056
22. Zhou H, Liu L, Yin K, Liu SL, Li GX (2006) Electrochem Commun 8:1168–1172
23. Cheng H, Scott K (2010) J Power Sources 195:1370–1374
24. Wang G, Sun G, Zhou Z, Liu J, Wang Q, Wang S, Guo J, Yang S, Xin Q, Yi B (2005) Electrochem Solid State Lett 8:A12–A16
25. Planeix JM, Coustel N, Coq B, Brotons V, Kumbhar PS, Dutartre R, Geneste P, Bernier P, Ajayan PM (1994) J Am Chem Soc 116: 7935–7936
26. Paulus UA, Schmidt TJ, Gasteiger HA, Behm RJ (2001) J Electroanal Chem 495:134–145
27. Freunberger SA, Chen Y, Peng Z, Griffin JM, Hardwick LJ, Barde F, Novak P, Bruce PG (2011) J Am Chem Soc 133:8040–8047
28. McCloskey BD, Bethune DS, Shelby RM, Girishkumar G, Luntz C (2011) J Phys Chem Lett 2:1161–1166
29. Balaish M, Kraytsberg A, Eli Y (2014) Phys Chem Chem Phys 16: 2801–2822
30. Zahoor A, Christy M, Jeon JS, Lee YS, Nahm KS (2015) J Solid State Electrochem 19:1501–1509
31. Lim HD, Park KY, Gwon H, Hong J, Kim H, Kang KS (2012) Chem Commun 48:8374–8376
32. Liu Z, Ling XY, Su X, Lee JY (2004) J Phys Chem B 108:8234–8240
33. Thamaphat K, Limsuwan P, Ngotawornchai B (2008) Kasetsart J Nat Sci 42:357–361
34. Zhang K, Zhang L, Chen X, He X, Wang X, Dong S, Han P, Zhang C, Wang S (2013) Gu L, Cui G. J Phys Chem C 117:858–865
35. Oh SH, Nazar LF (2012) Adv Energy Mater 2:903–910
36. Wang HL, Yang Y, Liang YY, Zheng GY, Li YG, Cui Y, Dai H (2012) J Energy Environ Sci 5:7931–7935
37. Laoire CO, Mukerjee S, Abraham KM (2009) J Phys Chem C 113: 20127–20134
38. Laoire CO, Mukerjee S, Abraham KM (2010) J Phys Chem C 114: 9178–9186
39. Conway BE, Liu TC (1990) Langmuir 6:268–276
40. Jerkiewicz G, Vatankhah G, Lessard J, Soriaga MP, Park YS (2004) Electrochim Acta 49:1451–1459
41. Reier T, Oezaslan M, Strasser P (2012) ACS Catal 2:1765–1772
42. Padbury R, Zhang X (2011) J Power Sources 196(10):4436–4444
43. Yang OB, Woo SI, Kim YG (1994) Appl Catal A 115:229–241
44. Sinfelt JH, Via GH (1979) J Catal 56:1–11
45. Karan HI, Sasaki K, Kuttiyel K, Farberow CA, Mavrikakis M, Adzic RR (2012) ACS Catal 2(5):817–824
46. Nie Y, Li L, Wei Z (2015) Chem Soc Rev 44(8):2168–2201